2018-01-0974

Adaptive Turbo Matching: Radial Turbine Design Optimization through 1D Engine Simulations with Meanline Model in-the-Loop

P.Kapoor and A.Costall - Imperial College London
N.Sakellaridis, R.Lammers and J.Hooijer - Mitsubishi Turbocharger and Engine Europe B.V.
S. Guilain and H.Tartoussi – Groupe Renault

Abstract

Turbocharging has become the favored approach for downsizing internal combustion engines to reduce fuel consumption and CO_2 emissions, without sacrificing performance. Matching a turbocharger to an engine requires a balance of various design variables in order to meet the desired performance. Once an initial selection of potential compressor and turbine options is made, corresponding performance maps are evaluated in 1D engine cycle simulations to down-select the best combination. This is the conventional matching procedure used in industry and is 'passive' since it relies on measured maps, thus only existing designs may be evaluated. In other words, turbine characteristics cannot be changed during matching so as to explore the effect of design adjustments. Instead, this paper presents an 'adaptive' matching methodology for the turbocharger turbine. By coupling an engine cycle simulation to a turbine meanline model ('in-the-loop'), adjustments in turbine geometry are reflected in both the exhaust boundary conditions and overall engine performance. Running the coupled engine-turbine model within an optimization framework, the optimal turbine design evolves. The methodology is applied to a Renault 1.2L turbocharged gasoline engine, to minimize fuel consumption over given full- and part-load operating points, while meeting performance constraints. Despite the current series production turbine being a very good match already, and with optimization restricted to a few turbine geometric parameters, the full-load case predicted a significant cycle-averaged BSFC reduction of 3.5 g/kWh, while the part-load optimized design improved BSFC by 0.9 g/kWh. No engine design parameters were changed, so further efficiency gains would be possible through simultaneous engine-turbocharger optimization. The proposed methodology is not only useful for improving existing designs; it can also develop a bespoke turbine geometry in new engine projects where there is no previously available match. For these reasons, 'adaptive' turbo matching will become the standard approach in the automotive industry.

Introduction

Turbocharging the gasoline passenger car engine is now commonplace in industry as part of the technology mix alongside gasoline direct injection (GDI) and downsizing, in the effort to lower fuel consumption and CO_2 emissions from personal transportation. The process of selecting a turbocharger for a particular customer engine application, known as turbocharger matching, is a critical step in being able to meet the desired performance characteristics. There is typically a trade-off between key end user requirements such as fuel economy versus driveability (the latter being a subjective combination of high power, fast transient response and especially 'good low-end torque') and this is strongly affected by turbocharger choice. The most suitable turbocharger configurations are identified by superimposing the target engine operation on characteristic compressor and turbine performance maps. The compressor options that provide adequate surge and choke margins while achieving high efficiency are selected first. Then the turbine options that meet the compressor power requirement with high efficiency and low inertia are chosen. Once this initial selection of potential compressor and turbine options has been made, the corresponding maps are evaluated in 1D engine cycle simulations (e.g., GT-POWER) to further down-select the turbocharger match that is predicted to best meet customer requirements.

This is the typical matching procedure used in the automotive industry, which takes place in the beginning of a turbocharger project. It may be reviewed and updated as more information becomes available (e.g., customer engine test data for model validation), but nonetheless sets the initial design direction and thus has important consequences for all that follows. The authors describe it as a 'passive' approach in the sense that it relies on knowing the aforementioned maps that have been previously measured on the hot gas bench, i.e., only existing turbocharger designs may be evaluated against engine project requirements. This means the performance characteristics of the selected turbine, for example, cannot be changed during the matching simulation in order to explore whether small geometrical changes would better match the particular engine flow conditions. On the other hand, while 3D CFD can be used to optimize a turbine aerodynamic design for given engine flow boundary conditions, this approach would not be consistent due to the highly-coupled nature of the engine-turbocharger system, i.e., any turbine design change would require a new set of boundary conditions. What's required instead is a framework that models both engine and turbine with acceptable accuracy and accounts for their coupling. This paper presents an 'active' or 'adaptive' matching methodology for the turbocharger turbine. By coupling an engine cycle simulation to a meanline model of the turbine's aerodynamic performance (i.e., 'in-the-loop'), the effect of turbine geometry changes will be reflected in the exhaust boundary conditions, as well as the overall engine performance prediction. Then, by running this coupled engine-turbine model within an optimization framework, the optimal turbine design will evolve.

A meanline model is a quasi-1D approach to predict the aerodynamic performance of, in this case, a radial turbine, using limited geometric parameters. It assumes there is a mean streamline through the turbine stage along which a number of calculation stations may be identified and which are representative of average flow conditions. This permits straightforward thermodynamic calculations of turbine performance using a minimum of geometric data. The main limitation, however, is the reliance on empirical loss correlations, which are necessary to estimate the magnitude of various sources of pressure loss and flow blockage [1]. Much of the classical work involving meanline modeling was performed at NASA [2,3], establishing the basic set of loss models to predict radial turbine performance. Baines [4] developed a meanline loss modeling system capable of predicting both the on- and off-design performance of radial turbines, as a refinement of the NASA approach. Qiu and Baines [1] extended the meanline calculation method into the high pressure ratio region of the turbine map and provided a method to obtain consistent predictions under subsonic, transonic or supersonic flow conditions. Abidat [5] used a meanline model to predict radial turbine performance in steady and pulsating flow conditions. Romagnoli and Martinez-Botas [6] developed a meanline model to predict performance of nozzled and nozzleless mixed flow turbines and validated their predictions against experimental data. Sakellaridis and Hountalas [7] developed a meanline model for simulation of turbochargers to support diagnostic investigations in diesel engines.

Following description of the methodology, the paper applies the proposed coupled engine-turbine optimization framework to a Renault 1.2L turbocharged gasoline passenger car engine. Having been developed over a number of generations, the current series production turbine supplied for this engine is already a very good match. Nonetheless, the turbine aerodynamic design is optimized over a number of steady-state engine operating points under both full- and part-load conditions while meeting certain constraints, starting with the current production geometry as the baseline. The corresponding engine model has been previously validated against measured engine dynamometer data, whilst the turbine meanline model is also shown to correctly predict performance of the baseline production turbine when compared against flow bench data.

Turbine Meanline Methodology

The meanline model in this work is based on the quasi-one dimensional procedure initially used by the authors in Ref. [8], which determines the flow state at (in this case) three different stations through the nozzleless radial turbine stage: 1) volute, 2) rotor inlet, and 3) rotor outlet, as shown in Figure 1. (N.B. a stage employing nozzles will require more stations [6].)

The meanline model accounts for energy dissipation along the flow path through the turbine stage by deploying a set of empirical correlations (or loss models) that describe loss generation. A common feature of most loss modeling systems is a conceptual division of the overall loss into separate components, corresponding to different physical loss mechanisms [4]. The first classification distinguishes volute and rotor losses – which are described next.

Volute loss modelling

As per Ref. [6], two major volute loss mechanisms are considered, embodied in the swirl and pressure loss coefficients. These account for irreversibilities due to mixing, secondary flow and recirculation.

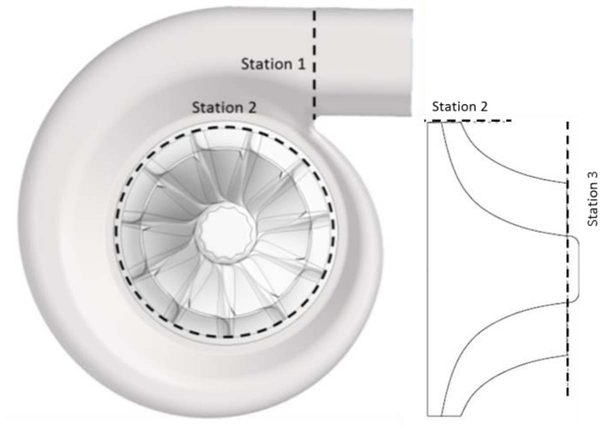

Figure 1. Stations for turbine meanline model calculation.

Swirl loss coefficient (S)

In an ideal volute, angular momentum of is conserved. In reality, some is lost due to wall friction between the flow and volute [9]. To account for this, the swirl loss coefficient S is introduced to the conservation of angular momentum in Equation 1, where C is the absolute velocity, C_θ the tangential velocity, and r the radius. Typical values range between 0.85–0.95 [10].

$$C_1 r_1 S = C_{\theta 2} r_2 \tag{1}$$

Pressure loss (K_{P})

The pressure loss coefficient, K_{P} (Equation 2), models the pressure (P) losses due to volute wall friction [11]; typical values lie in the range 0.1–0.3 [10].

$$K_{\mathrm{P}} = \frac{P_{01} - P_{02}}{P_{02} - P_2} \tag{2}$$

Rotor loss modeling

Energy losses in the rotor are modeled according to the NASA approach [2,3], which attributes losses due to incidence effects, friction in the flow passage, clearance between rotor and shroud, and disk friction on the wheel.

Incidence loss (L_{i})

Ideal flow conditions at rotor inlet do not actually correspond to perfect alignment between the flow and the blade. This phenomenon has been demonstrated experimentally by Yeo and Baines [12] and is due to the pressure difference between the blades' pressure and suction surfaces. In a radial turbine, this results in an optimum relative inlet flow angle, $\beta_{2,\mathrm{opt}}$, of somewhere between -20° to -30° [10]. The incidence angle, i_2, is defined in the meanline model as the difference between the actual and optimum relative inlet flow angles (Equation 3), i.e., the ideal situation is when $i_2 = 0$. (N.B. other works refer the incidence angle to the blade angle; both definitions are in general use and so care must be taken to be consistent.)

$$i_2 = \beta_2 - \beta_{2,\mathrm{opt}} \tag{3}$$

As the relative inlet flow angle departs from the optimum (i.e., i_2 becomes non-zero), flow separation becomes more likely and mixing losses in the rotor increase [11]. The enthalpy loss due to incidence, L_i (Equation 4), is modeled assuming that the change in relative tangential kinetic energy manifests as an increase in internal energy of the gas (and a consequent increase in entropy). Here K_i is the incidence loss coefficient and W_2 is the relative inlet velocity.

$$L_\mathrm{i} = 0.5\ K_\mathrm{i}\ W_2^2\ \sin^2 i_2 \tag{4}$$

Clearance loss (L_c)

There must exist a clearance between the blade tip and the shroud, the latter provided by the inside of the turbine housing (in a typical turbocharger). The pressure difference between the pressure and suction blade surfaces drives a tip clearance flow through this gap, resulting in an enthalpy loss. This clearance loss, L_c, is based on that in Ref. [4], shown here in Equation 5

$$L_\mathrm{c} = \frac{U_2^3\ N}{8\pi}\left(K_\mathrm{a} e_\mathrm{a} C_\mathrm{a} + K_\mathrm{r} e_\mathrm{r} C_\mathrm{r} + K_\mathrm{ar}\sqrt{e_\mathrm{a} C_\mathrm{a} e_\mathrm{r} C_\mathrm{r}}\right) \tag{5}$$

where

- U_2 is the inlet blade speed;
- N is the blade number;
- K_a and K_r are resp. axial and radial clearance loss coefficients;
- e_a and e_r are axial and radial tip clearances, resp.;
- K_ar is the cross-coupling coefficient; and

where the axial and radial absolute velocities, resp. $C_\mathrm{a}$and C_r, are

$$C_\mathrm{a} = \frac{1-\left(\frac{r_{3,\mathrm{tip}}}{r_2}\right)}{C_{\mathrm{r},2}\ b_2} \tag{6}$$

and

$$C_\mathrm{r} = \left(\frac{r_{3,\mathrm{tip}}}{r_2}\right)\frac{z-b_2}{C_{\mathrm{a},3}\ r_3\ b_3} \tag{7}$$

Passage loss (L_p)

Passage loss accounts for pipe friction and blade loading losses in the blade passage. The meanline model uses the treatment from Ref. [10], described here in Equation 8, where K_p is the passage loss coefficient and W_3 is the relative outlet velocity.

$$L_\mathrm{p} = 0.5\ K_\mathrm{p}\left(W_2^2 \cos^2 i_2 + W_3^2\right) \tag{8}$$

Disk friction loss (L_df)

The disk friction or windage loss, L_df, accounts for friction on the backface of the turbine wheel. The meanline model employs the expression in Ref. [3], shown here in Equation 9, where ρ_2 is the rotor inlet gas density, $\dot{m}$ its mass flow rate, and μ its dynamic viscosity.

$$L_\mathrm{df} = \frac{0.02125\ U_2^3\ \rho_2^2}{\dot{m}\left(\frac{\rho_2\ U_2\ r_2}{\mu}\right)^{0.2}} \tag{9}$$

The meanline model has been programmed in FORTRAN, and requires the turbine rotational speed, total inlet conditions, static outlet pressure, the thermodynamic properties of the working medium, and the basic turbine geometric parameters as inputs. The model returns the mass flow rate and total-to-static efficiency as outputs.

Turbine Meanline Model Validation

Experimental validation

As a validation exercise, the meanline model was used to predict the performance of an off-the-shelf, ~36mm diameter radial turbine for a mass-produced passenger car engine turbocharger, manufactured by Mitsubishi Turbocharger and Engine Europe BV (MTEE). First of all, the model is calibrated against a single speed line from the measured turbine map, using a genetic algorithm (GA) to obtain the coefficients for the different loss mechanisms, with the objective of minimizing the sum of squares between the model prediction and experimental data. Once calibration was attained for this single speed line, the model was exercised to predict turbine performance for the remaining four speed lines in the measured map. Figure 2 compares the measured and predicted swallowing capacity, while Figure 3 compares the efficiency, for the five speed lines. Here, rotational speed has been normalized against the maximum measured speed; the speed line used for calibration is labelled '100% Speed'.

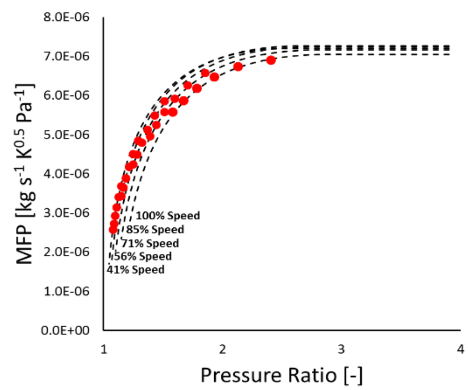

Figure 2. Comparison of measured and predicted turbine swallowing capacity.

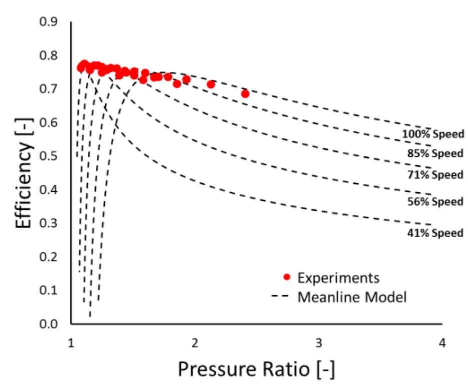

Figure 3. Comparison of measured and predicted turbine efficiency.

It can be seen that the calibrated model predicts the turbine behavior very well both in terms of mass flow and efficiency within the measured data range. However, since the model predicts turbine performance over a considerably wider range of pressure ratio compared to that available from gas stand measurements, it does mean the meanline model cannot be validated against experimental data in these regions – this issue will be addressed in the next section.

When employing the turbocharger compressor as the loading device during map measurement, the measured turbine speed lines will be quite limited in width due to compressor surge and choke. This width does not sufficiently cover the range of turbine operation on-engine, and so when used in 1D engine cycle simulations, such measured maps must be extrapolated, using a mathematical or physics-based technique, or a combination thereof. Nevertheless, that approach will likely have a weaker physical basis than using the meanline model presented here, resulting in poorer turbine performance prediction when the engine operates away from the measured map.

CFD validation

To ascertain the predictive accuracy of the meanline model outside of the map measured map range, a 3D CFD analysis of the same subject turbine was performed. The meanline model predictions were compared against corresponding predictions obtained from CFD.

CFD setup and pre-processing

The 3D geometry of the turbine volute and rotor was provided by MTEE for the CFD analysis. A preliminary step was to obtain a clean geometry prior to meshing, i.e., removal of feature details that are irrelevant for CFD analysis and which would potentially impose unnecessarily high local mesh resolution. Altair HyperMesh was then used to mesh the entire fluid domain: turbine volute, rotor, plus inlet and outlet extrusions, as shown in Figure 4.

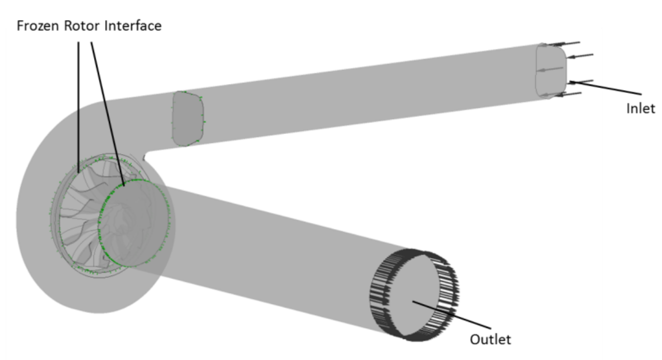

Figure 4. Turbine stage CFD domain and boundary conditions.

An unstructured mesh (Figure 5) was created for all components, with 10 elements in the near wall boundary layer mesh. An average y^+ value of 5 was achieved. The grid consisted of 2.1 million elements in the volute and 3.2 million elements in the rotor. 3D RANS steady-state simulations were carried out using the ANSYS CFX 18.1 finite volume solver. The two-equation k-ω SST turbulence model was selected; this combines the robust formulation of the k-ω model in the near wall region with the far stream independence of the k-ε model [13]. It provides more accurate predictions when there is flow separation under adverse pressure gradients and in cases of wall bounded flows [14].

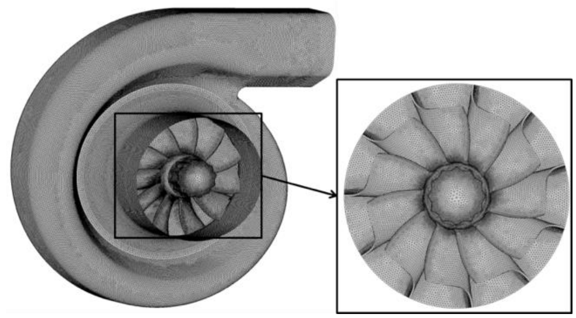

Figure 5. Computational mesh of turbine volute and rotor.

A total pressure of 150 kPa and total temperature of 373.15K were applied as the inlet boundary conditions at the plane identified in Figure 4, together with a medium turbulent intensity of 5%, for all simulations. Total-to-static efficiency and mass flow rate were monitored to track convergence, with a convergence criterion of $1\text{x}10^{-5}$ used for all residuals. Static pressure was specified as the outlet boundary condition, and was varied to obtain different operating conditions. The rotor shroud was defined as a counter rotating wall to simulate the relative motion between the turbine rotor and volute. As shown in Figure 4, frozen rotor interfaces were specified between the stationary volute and rotor, and between the rotor and outlet duct. All walls were defined as adiabatic.

Comparison of CFD and meanline predictions

Figure 6 compares the predictive capability of the meanline model against the CFD simulations, for three speed lines.

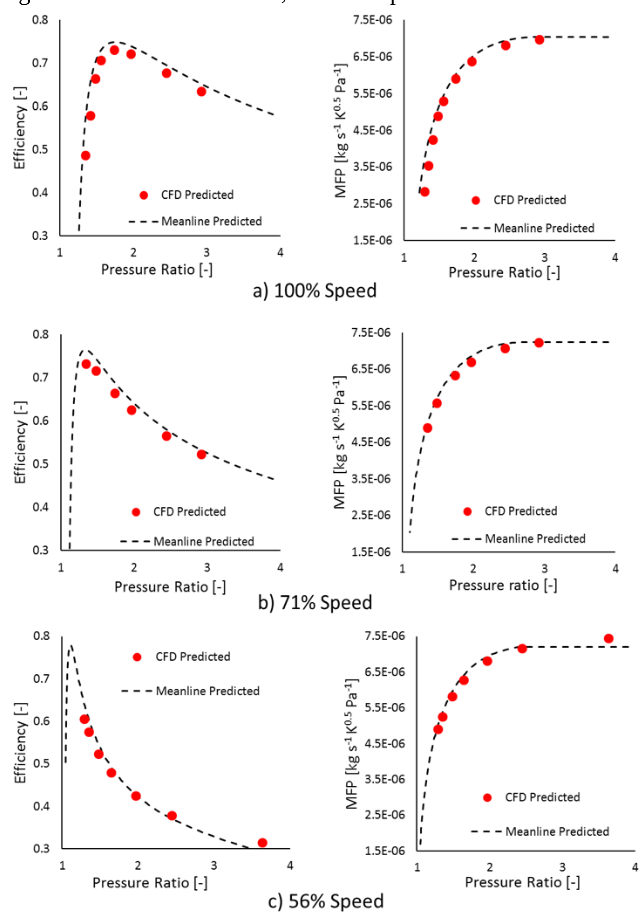

Figure 6. Comparison of 3D CFD and meanline model predictions.

The meanline model swallowing capacity and efficiency predictions agree well with CFD (within ± 3%-age points), with trends captured for all three speed lines (not only at the 100% speed used for calibration), even at very low and high pressure ratios (where test data isn't available). Combined with the earlier experimental validation, this gives confidence that the meanline model will provide accurate turbine performance prediction across the full operating range experienced in 1D engine simulations.

Engine Model Validation

A Renault 1.2L turbocharged GDI engine (Table 1) was used as the subject engine in this study. The engine air system employs a fixed geometry, wastegated turbocharger supplied by MTEE. The wastegate is used to control the delivered boost pressure by increasing the effective exhaust flow area, bypassing some exhaust gas around the turbine, restricting the developed turbine power.

Table 1. Renault 1.2L turbocharged GDI engine specifications.

Capacity (cc)	1198	Combustion system	4-stroke GDI
No. of cylinders	4		
Bore x stroke (mm)	72.2 x 73.1	Air system	Single, fixed geometry, wastegated turbocharger
Compression ratio	10:1		

A GT-POWER 1D engine cycle simulation model was supplied by the engine manufacturer for this study. Measured compressor and turbine performance maps, provided by MTEE, were used for modeling the turbocharger at this stage. The engine model targets the desired torque at each speed using the in-built wastegate controller. Validation was carried out for 14 full-load steady-state operating points (Table 2) against engine dynamometer test data.

Table 2. Full-load engine operating points.

Engine speed (rpm)	Normalized target engine torque	Engine speed (rpm)	Normalized target engine torque
1000	0.65	3000	1.00
1250	0.83	3500	1.00
1500	1.00	4000	1.00
1750	1.00	4500	0.95
2000	1.00	5000	0.85
2250	1.00	5500	0.78
2500	1.00	6000	0.71

All results in the paper have been normalized by the maximum value of the corresponding parameter. Figure 7 presents the comparison of simulated engine performance against the engine test data. It can be seen in Figure 7 (a) that the engine model predicts brake power well across the speed range; however, when translated into brake torque any small differences, particularly at low engine speeds, are amplified. Indeed, Figure 7 (b) shows that the model over predicts the torque at the third and fourth engine speeds. Similarly, Figure 7 (c) shows the trend of brake specific fuel consumption (BSFC), which is the preferred indicator of overall system efficiency in this paper, is well-captured except at the lowest engine speeds.

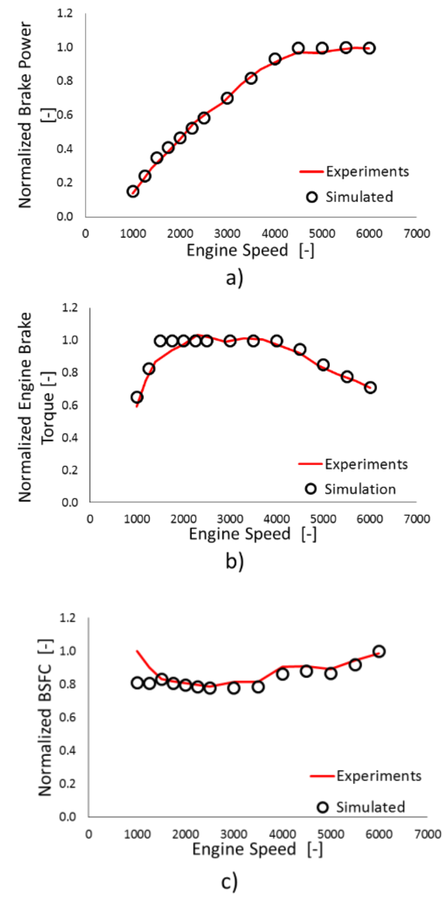

Figure 7. Comparison of measured and simulated engine performance.

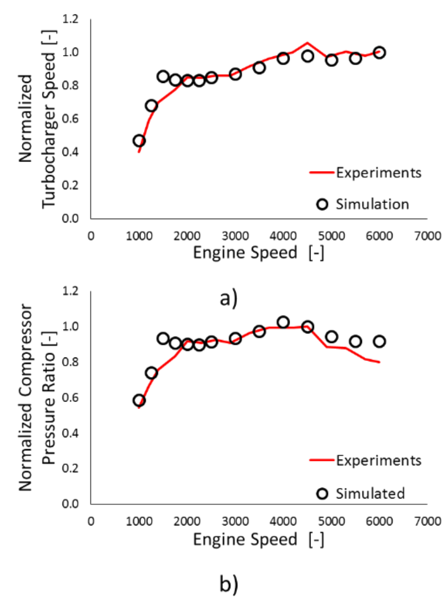

Figure 8. Comparison of measured and simulated turbocharger performance.

Figure 8 compares the predicted cycle-averaged turbocharger performance against test data. In Figure 8 (a), the engine model predicts turbocharger speed reasonably well over the entire measured range, again except for engine speeds between 1500–2000 rpm. However, in Figure 8 (b), the compressor pressure ratio (thus boost) is well-predicted only for the mid-speed range (2000–4500 rpm). At high engine speeds (5000–6000 rpm), the model predicts too high a boost, in order to meet the required engine torque. Despite the deviations between simulated and measured engine performance (mainly at low and high engine speeds), cycle-averaged predictions can be used to evaluate relative engine performance.

Turbine Modeling: Map versus Meanline

As mentioned, 1D engine cycle simulation tools conventionally use experimentally-measured turbine and compressor maps in order to simulate turbocharger performance. Due to measured width limitations, turbine maps especially must usually be extrapolated before they can be used in such simulations, thereby introducing a certain amount of prediction inaccuracy [7], especially when operating far outside the measured range [15]. The long-term objective of this work is to reduce this modeling uncertainty and reliance on the measured turbocharger turbine maps for engine simulations. Thus the radial turbine meanline model was integrated with the engine model to predict turbine behavior, supplanting the turbine map component. (Compressor performance prediction suffers less from extrapolation, and continued to be modeled using maps.) In an engine simulation, the instantaneous turbocharger rotational speed is known, while turbine expansion ratio and thermodynamic fluid properties are defined by the instantaneous pressure and temperature conditions in adjoining ducts. At every time step, these are provided as boundary conditions to the meanline model, which in turn supplies its prediction of instantaneous turbine mass flow and efficiency.

To assess how the choice of map-based or meanline-based turbine modeling affects performance prediction, 1D engine simulations were performed for both approaches, for the 14 full-load engine operating points in Table 2, and 8 additional part-load points listed in Table 3.

Table 3. Part-load engine operating points.

Engine speed (rpm)	Normalized target engine torque	Engine speed (rpm)	Normalized target engine torque
1500	0.85	2500	0.80
1500	0.75	2500	0.85
2000	0.85	3000	0.75
2000	0.75	3500	0.60

Figure 9 compares the engine model full-load predictions using the two turbine simulation methods: map-based and meanline model. It can be seen in Figure 9 (a) and Figure 9 (b) that the meanline model-based simulation predicts the same engine torque and power as the map-based simulation. The BSFC predictions in Figure 9 (c) match well between methods at low and mid-engine speeds, however at the highest engine speed the meanline model-based simulation shows a 1.2% lower BSFC than the map-based prediction. This can be explained by looking at the PMEP predictions for the two cases in Figure 9 (d), where the turbine meanline model results in improved (less negative) pumping work and hence lower BSFC. Turbocharger speed and compressor operation were identical between methods.

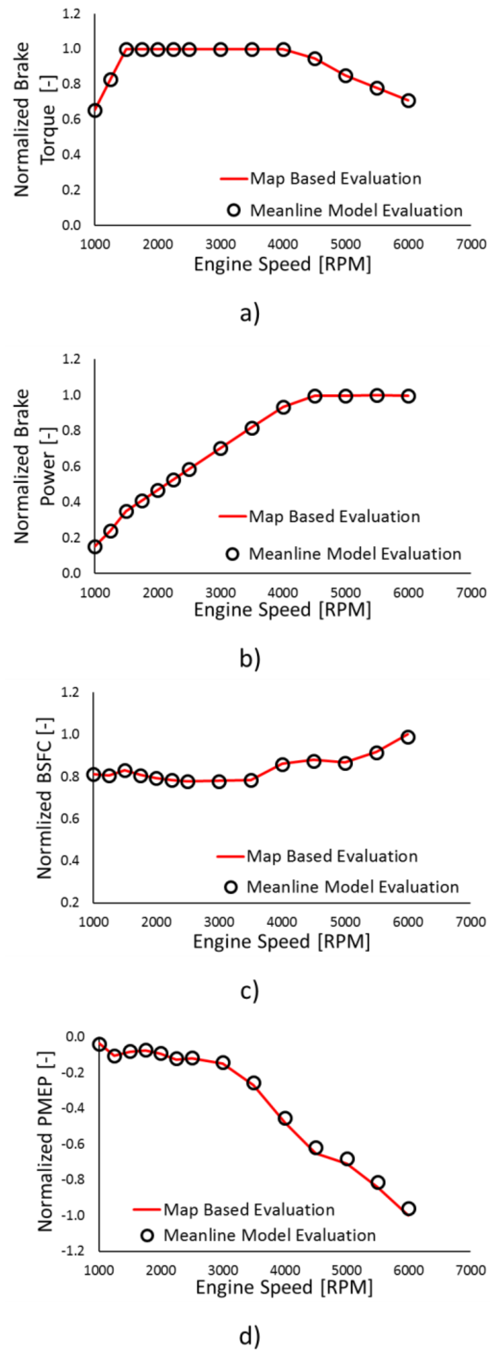

Figure 9. Map vs meanline turbine models: full-load engine performance.

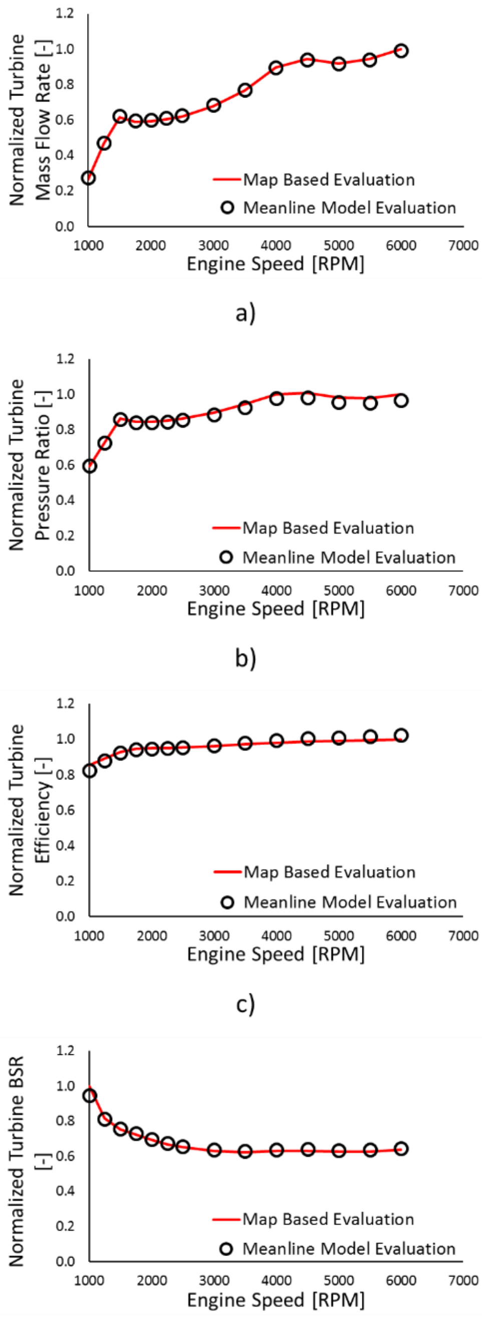

Figure 10. Map vs meanline turbine models: turbine operation at full load.

Figure 10 continues the comparison of map- and meanline-based turbine modeling options, at the turbine level. Both estimate very similar turbine mass flow rate and blade speed ratio (BSR), in Figure 10 (a) and Figure 10 (d) resp., at all engine speeds. Pressure ratio and efficiency are also similarly predicted except at the highest engine speeds where there is a ~2.5% difference. This is likely due to the extrapolation required in this operating region.

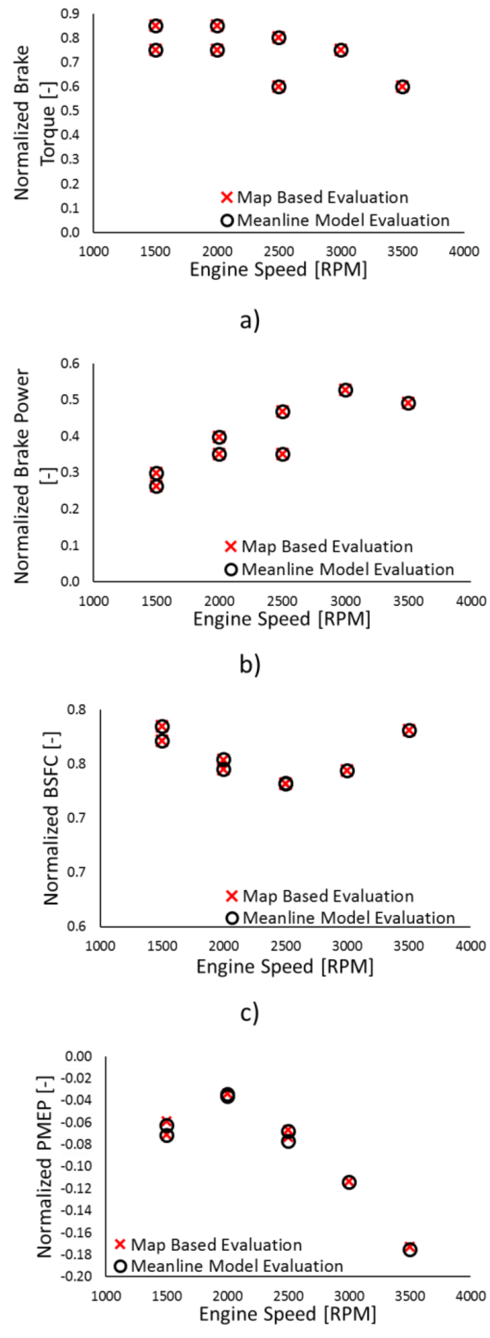

Figure 11. Map vs meanline turbine models: part-load engine performance.

Next, predictions at the part-load engine operating points in Table 3 are compared. Figure 11 shows both methods again predict similar engine performance, in terms of brake power, torque and BSFC. It can be seen from Figure 12 (a) and Figure 12 (c) that the meanline model-based simulation predicts slightly higher mass flow through the turbine and lower efficiency at the same engine speed, compared to the map-based approach. Since these parameters have an opposite effect on pumping work, they balance each other out, and so the predicted BSFC remains similar (Figure 11 (c)). The deviation in mass flow and efficiency predictions may again be attributed to extrapolation effects in the map-based approach.

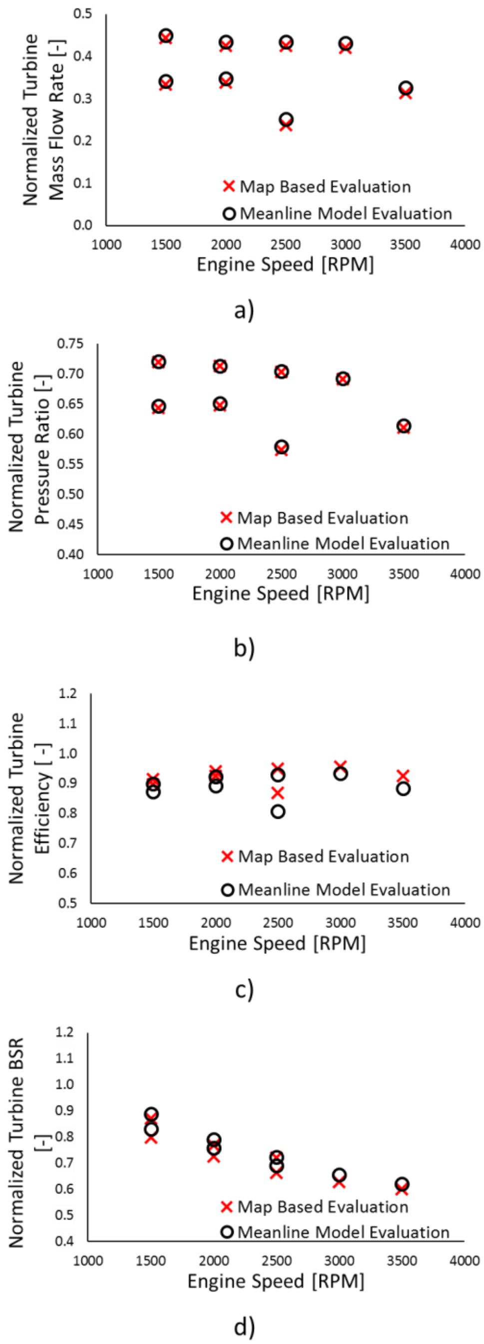

Figure 12. Map vs meanline turbine models: turbine operation at part load.

Turbine Optimization to Reduce System BSFC

The coupled engine-turbine meanline model permits 1D turbocharged engine simulations without recourse to measured turbine maps, instead relying on a description of the turbine geometry (plus, of course, calibrated loss correlations). And since the geometry may be adjusted during simulation, it becomes a suitable platform for performing aerodynamic optimization. A genetic algorithm [16] was selected for this purpose, a type of evolutionary algorithm [17] inspired by biological processes (e.g., mutation, crossover, natural selection), variously applied in turbomachinery design to iteratively improve a set of solution candidates [e.g., 18, 19].

In this work, the GA optimizer available in the 1D engine cycle simulation software GT-POWER was used. Figure 13 shows the basic turbine geometric parameters. Table 4 lists the parameters to be varied by the optimizer – a maximum perturbation of ±8% to the nominal values was allowed (to limit the change in turbine wheel inertia). A population size of 30 was specified, which is more than twice the number of design variables, as recommended by Ref. [18]. A crossover rate of 1, a crossover rate distribution index of 15, and a mutation rate of 0.14 were specified to create diversity in the population. The scope of optimization was purposely limited to the turbine, i.e., no compressor or engine model parameters were changed. The objective was to minimize overall system BSFC over a set of (1) full- and (2) part-load steady-state engine operating points.

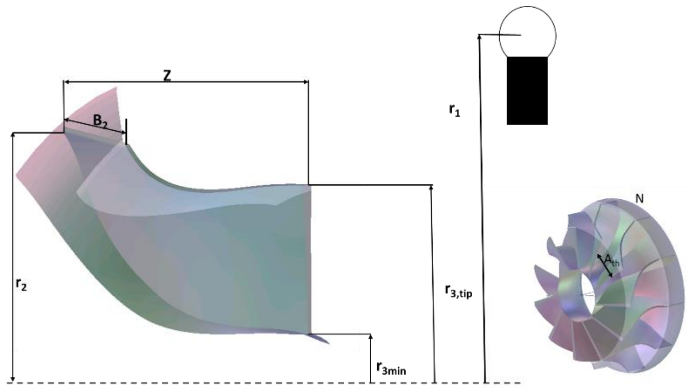

Figure 13. Basic turbine geometric parameters.

Table 4. Turbine geometric parameters varied by the optimizer.

Parameter	Description
A_1	Volute inlet area
r_1	Volute inlet radius
B_2	Rotor inducer height
r_2	Rotor inlet radius
z	Blade length
$r_{3,tip}$	Rotor outlet tip radius
β_{3b}	Rotor outlet blade angle

Case 1: Full-load turbine design optimization

This case considered an imagined steady-state drive cycle, comprising a sub-set of 6 full-load engine operating points (Table 5), over which turbine aerodynamic optimization was performed. Here, these were given equal importance, but it is straightforward to assign weightings to distinguish different drive cycles.

Table 5. Full-load engine operating points for turbine optimization (Case 1).

Engine speed (rpm)	Normalized target engine torque	Engine speed (rpm)	Normalized target engine torque
1250	0.83	3500	1.00
1500	1.00	4500	0.95
2250	1.00	6000	0.71

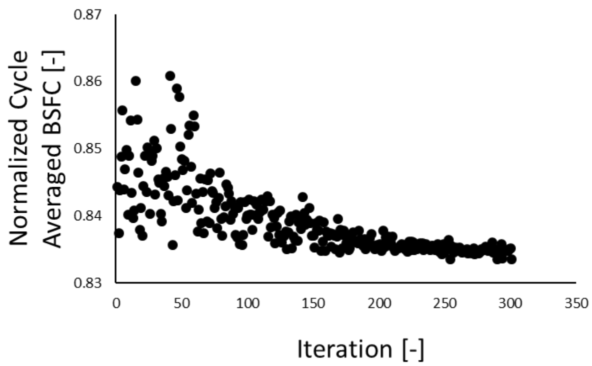

Figure 14. Optimization convergence at full load (Case 1).

Figure 14 shows the convergence plot for the optimization process, which is halted once the change in objective function (i.e., BSFC) is less than < 0.05 g/kWh. In Case 1, after ~300 iterations (~6 days on a workstation using two cores of an i7-2600 processor, clock speed 3.4 GHz), the optimizer achieved an improvement in the cycle-averaged BSFC of ~3.5 g/kWh, a significant reduction.

Investigating further, Table 6 presents the relative change in the optimized design parameters compared to the baseline design. It can be seen that Case 1 optimization resulted in an increase in the volute inlet area A_1, the rotor inducer height B_2, the rotor inlet radius r_2, and the rotor outlet tip radius $r_{3,\mathrm{tip}}$, but a decrease in the volute inlet radius r_1, the rotor outlet blade angle $\beta_{3\mathrm{b}}$, and the blade length z.

Table 6. Relative change in design parameters optimized at full load (Case 1).

Parameter	Description	Change relative to baseline (%)
A_1	Volute inlet area	7.12
r_1	Volute inlet radius	-6.18
B_2	Rotor inducer height	4.04
r_2	Rotor inlet radius	7.38
z	Blade length	-2.44
$r_{3,\mathrm{tip}}$	Rotor outlet tip radius	6.73
$\beta_{3\mathrm{b}}$	Rotor outlet blade angle	-6.71

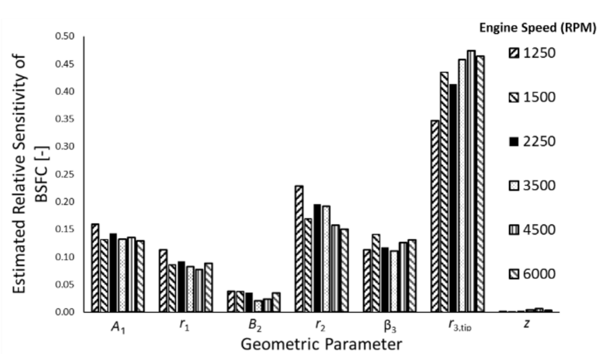

Figure 15. Influence of turbine geometric parameters on engine BSFC at different full-load engine speeds (Case 1).

Next, optimization data was used to explore the influence of individual turbine geometric parameters on engine BSFC, shown in Figure 15, where the shaded bars represent different engine speeds. Sensitivity is computed by a linear least squares approach using all iteration data. The slopes determined by least squares fitting are normalized by the sum of all slopes [20].

Straightaway it may be inferred that, in this case, blade length z has little influence on BSFC, while the rotor outlet radius $r_{3,\mathrm{tip}}$ shows the greatest influence, irrespective of engine speed. This can be related to the variation of turbine throat area with rotor outlet radius, which dictates swallowing capacity. The rotor inlet radius r_2 also has a significant impact on engine BSFC. The rotor outlet blade angle $\beta_{3\mathrm{b}}$ is the next most important design parameter. The volute parameters A_1 and r_1 also influence BSFC as they determine the turbine '*A*/*R*', a parameter used in the industry to denote relative turbine housing size. For example, a smaller *A*/*R* will tend to raise exhaust back pressure, consequently increasing pumping work and overall BSFC. Finally, while there is some variance in sensitivity to the same parameter between engine speeds, this is much smaller than sensitivity differences between parameters. Although brief, this analysis helps identify influential turbine design parameters, translating adjustments at the turbine component level to overall engine system level BSFC.

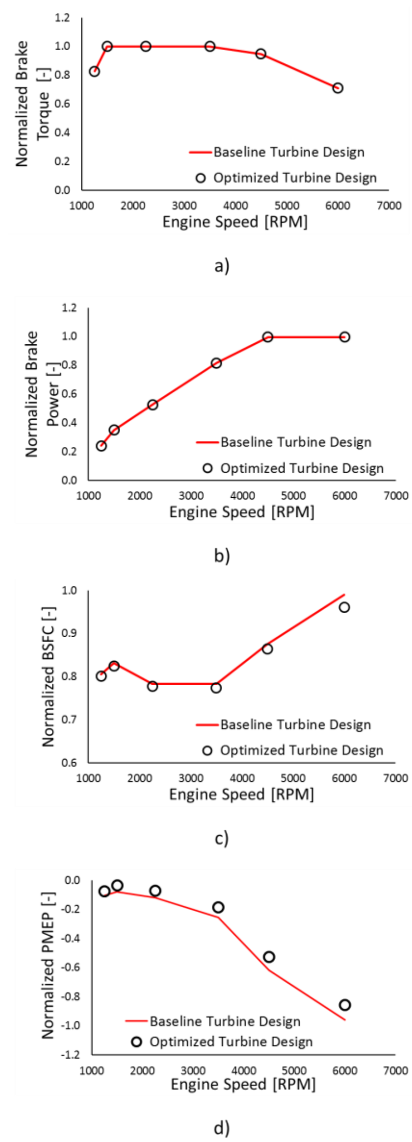

Figure 16. Comparison of full-load engine performance for baseline and optimized turbine designs (Case 1).

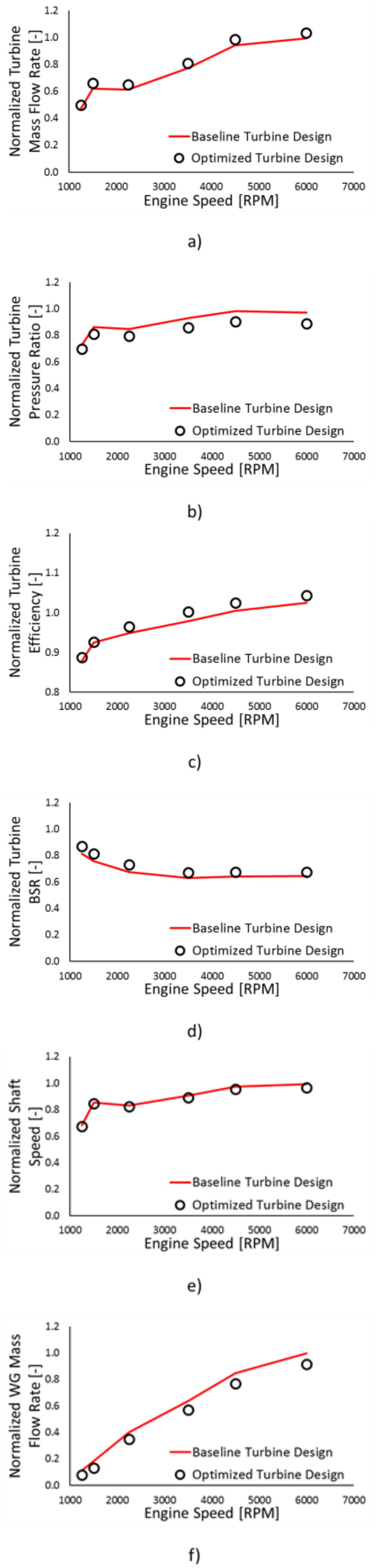

Figure 17. Comparison of turbine performance at full-load for baseline and optimized turbine designs (Case 1).

Figure 16 compares predicted engine performance for the baseline and optimized turbine designs. Figure 16 (a) and Figure 16 (b) simply confirm that the optimized design meets the torque and power targets. Figure 16 (c) shows the magnitude of BSFC reduction is larger at higher engine speeds, but there is an improvement at all speeds. This stems from improved (less negative) pumping work, as seen in Figure 16 (d), which can itself be explained by comparing the turbine operation in Figure 17.

Figure 17 (a) and Figure 17 (c) indicate that design optimization resulted in a turbine with improved flow capacity and efficiency at all engine operating points, while imposing a lower expansion ratio (Figure 17 (b)). This reduces exhaust back pressure and hence pumping work, reflected in improved BSFC. At the turbine stage level, improved efficiency may be attributed to the optimized design operating closer to the optimum BSR of ~0.7 for an ideal radial turbine [10], at least at the three highest engine speeds. Indeed, Figure 17 (d) shows that the optimized design operates at a slightly higher BSR at all engine speeds. Compressor operation for both designs remained the same; this is to be expected since the same compressor map is used, and, ignoring any slight differences in cylinder scavenging, the same nominal boost level will be required to meet the target torque. It follows then that, as shown in Figure 17 (e), turbocharger rotational speed remains almost identical for the two designs. Figure 17 (f) shows wastegate mass flow rate reduces compared to the baseline design, in order for the turbine to meet the power demanded by the compressor for the required boost pressure.

So, despite the current series production turbine already being a good match, and with optimization restricted to a handful of parameters, simulation results suggest there remains a worthwhile margin of 3.5 g/kWh for system efficiency gains at full load.

Case 2: Part-load turbine design optimization

Table 7 lists the 5 part-load engine operating points for which the second optimization case was performed. Again, each point was assigned equal importance in the absence of detailed drive cycle data.

Table 7. Part-load engine operating points for turbine optimization (Case 2).

Engine speed (rpm)	Normalized target engine torque	Engine speed (rpm)	Normalized target engine torque
2000	0.75	3000	0.75
2250	0.75	3500	0.60
2500	0.80		

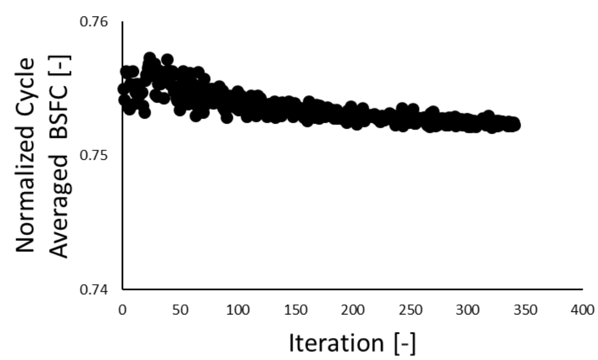

Figure 18. Optimization convergence at part load (Case 2).

The same GA configuration and parameter list as described for full-load optimization was again used, with convergence achieved after ~350 iterations (Figure 18). Table 8 shows the relative change in the design parameters as a result of optimization at part load, resulting in an increase in the volute area A_1, the rotor inlet radius r_2, and the rotor outlet tip radius $r_{3,\text{tip}}$. A decrease is seen in the volute inlet radius r_1, the rotor inducer height B_2, the rotor outlet blade angle $\beta_{3\text{b}}$, and the blade length z. The direction of these changes is the same as for the full-load case (except for rotor inducer height B_2, which increased by ~4% under optimization at full load). Nonetheless the small changes in magnitude go to show that the optimal turbine design does differ slightly between full- and part-load operation.

Table 8. Relative change in design parameters optimized at part load (Case 2) compared to those at full load (Case 1).

Parameter	Change relative to baseline (%)	
	Full load (Case 1) for comparison	Part load (Case 2)
A_1	7.12	7.66
r_1	-6.18	-5.30
B_2	4.04	-0.17
r_2	7.38	7.08
z	-2.44	-3.77
$r_{3,\text{tip}}$	6.73	7.32
$\beta_{3\text{b}}$	-6.71	-5.82

Figure 19 presents the sensitivity of BSFC to each design parameter, for the part-load optimization. Compared with Case 1 (full load), now both the rotor outlet blade angle $\beta_{3\text{b}}$ and the rotor outlet tip radius $r_{3,\text{tip}}$ show considerable influence on engine BSFC, at all engine speeds. Part-load BSFC is also sensitive to volute inlet area and radius. Rotor inducer height has a small influence on BSFC, as for the full-load case. Lastly, the blade length z continues to play a very minor role in determining engine BSFC.

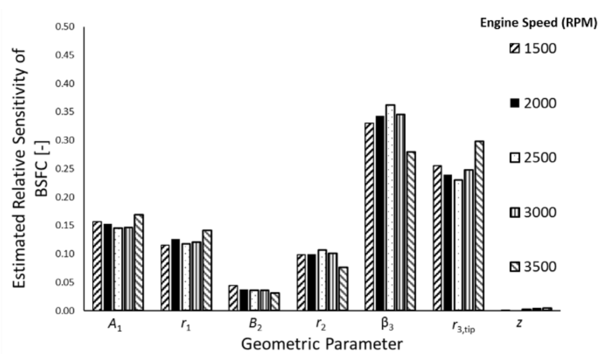

Figure 19. Influence of turbine geometric parameters on engine BSFC at different part-load engine speeds (Case 2).

Figure 20 compares predicted engine performance for the baseline and part-load optimized turbines. Figure 20 (a) and Figure 20 (b) again confirm that the optimized design meets the desired part-load torque and power. In Figure 20 (c), the optimized design improves the BSFC at all points, resulting in a slightly better cycle-averaged fuel consumption of 0.9 g/kWh overall. Again there appears to be some room to improve part-load engine efficiency through turbine optimization, albeit to a lesser extent that at full load.

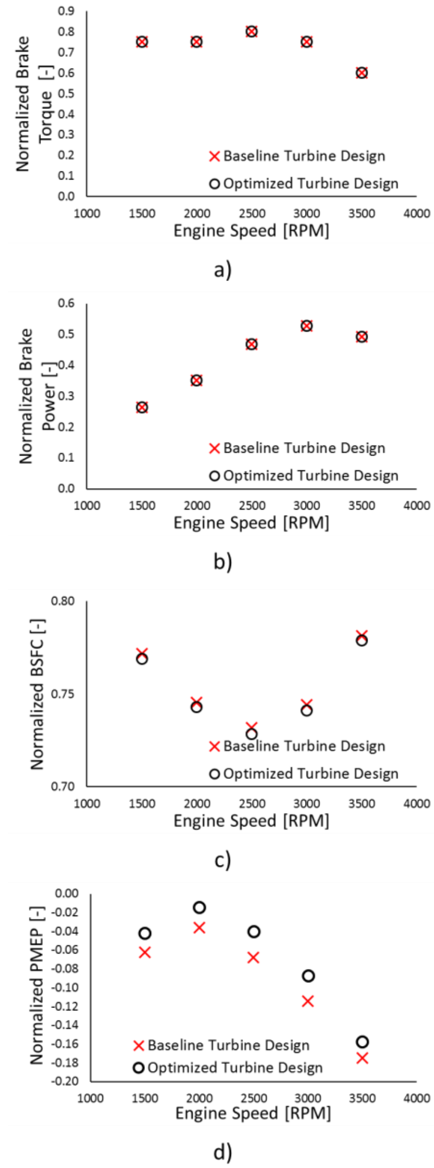

Figure 20. Comparison of part-load engine performance for baseline and optimized turbine designs (Case 2).

Figure 21 compares optimized and baseline turbine performance at part load. As for full load, both mass flow and efficiency increase (Figure 21 (a) & (c) resp.), while expansion ratio (Figure 21 (b)) decreases for the optimized design. Optimization again results in a design that operates at higher BSR (Figure 21 (d)), turbocharger rotational speed (Figure 21 (e)) remains constant, and wastegate flow (Figure 21 (f)) reduces to match the required compressor power.

Conclusions

This paper presents an 'adaptive' turbine matching methodology that couples a turbine meanline model to a 1D engine model. The turbine meanline model is based on existing loss correlations in the literature, and is first calibrated against a single speed line from a measured turbine map. Using the baseline series production turbine, validation of the meanline model against both experimental data and CFD provides confidence that the meanline model accurately predicts turbine performance across the full on-engine operation range.

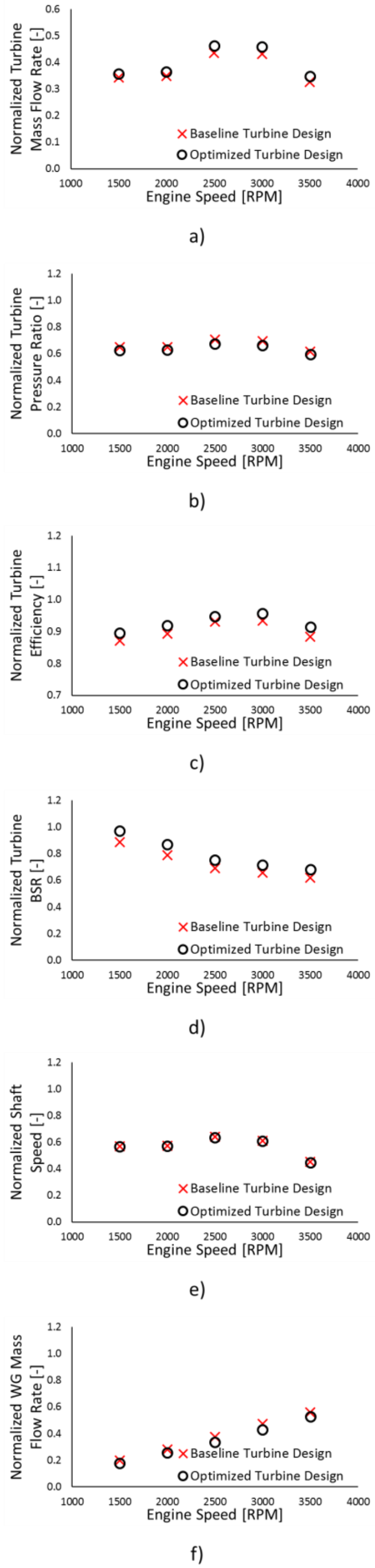

Figure 21. Comparison of turbine performance at part load for baseline and optimized turbine designs (Case 2).

The meanline model was coupled to an engine model for a Renault 1.2L turbocharged GDI passenger car engine, which was generally a good match to the engine dynamometer test data. Validation of the coupled engine-turbine model results in the same engine performance given the same baseline turbine design. A comparison of engine performance predictions using both map-based and meanline turbine models highlighted some differences, particularly in regions expected to suffer from turbine map extrapolation.

The main objective of the current paper is to demonstrate the use of a meanline model to optimize turbine design, in a scenario where the objective is to minimize fuel consumption over a given set of engine operating points. Two cases were considered: full- and part load, with all points given equal importance in each. In the full-load case, the GA-optimized turbine geometry predicted a significant reduction in cycle-averaged BSFC of 3.5 g/kWh. However, it should be noted that real passenger car drive cycles spend the clear majority of the time under part load conditions. In this case, the part-load optimized design showed just a 0.9 g/kWh cycle-averaged BSFC improvement – this is nonetheless worth having. Though it must also be noted that this was achieved with optimization restricted to a handful of turbine geometric parameters, and without any modification to the engine design or breathing and combustion control parameters (e.g., valve timing and spark advance). This suggests greater efficiency gains may be possible if engine and turbocharger optimization is performed simultaneously. Overall then, there appears to be attainable system-level efficiency benefits through turbine aerodynamic optimization.

The paper also briefly examined the influence of turbine design parameters on engine BSFC, using the data generated by the optimization process. This highlighted that, for the turbine design parameters under investigation:

- The most influential were the rotor outlet tip radius $r_{3,\mathrm{tip}}$ at full load, and the rotor outlet blade angle $\beta_{3\mathrm{b}}$ (closely followed by $r_{3,\mathrm{tip}}$) at part load;
- The least influential was the blade length z in either case; and
- There is a noticeable but less critical variation in the influence of each parameter across different engine speeds.

In sum, the benefits of ‘adaptive’ turbine matching by employing a coupled engine-turbine meanline model are that:

- It removes reliance on measured turbine maps (and the associated poor predictive accuracy incurred by map extrapolation);
- It enables aerodynamic optimization of an existing turbine geometry, or development of a bespoke turbine geometry in new engine projects where there is no previously available match, for given engine-level customer objective(s), e.g., BSFC; and
- It permits sensitivity of *engine-level* performance (including BSFC) to *component-level* design parameters (the turbine, in this case) to be studied.

The cost of these benefits is the not insignificant computational time required for an optimized turbine design to evolve. However, this must be weighed against the total time taken by the standard matching approach in which any number of turbine maps may need to be evaluated before the most suitable (though non-optimal) turbine design reveals itself. Based on their experience, the authors suggest that an ‘adaptive’ turbine matching process will in reality take no longer, yet will likely result in better designs. For these reasons, it is expected that some form of adaptive turbocharger matching will eventually become the standard approach.

Future work

The following items remain to be addressed:

- The current geometry optimization process is constrained to generate purely radial designs. This will be relaxed in future work to allow mixed flow designs to be evolved, in order to explore further efficiency improvements that are potentially on offer.
- The current work used an imagined set of full- and part-load engine operating points, and considered them separately, resulting in slightly different designs. This goes to show that the optimal turbine design differs between full- and part-load operation, and in general between any non-identical set of engine operating points. Hence future work will move towards turbine optimization over more realistic drive cycles, which will inherently comprise a mixture of full- and part- load operation.
- In the current work, optimization relies on the accuracy of the meanline model. While it has been validated against both test data and CFD for an existing design, future work must consider the corresponding optimized 3D geometry and its simulation in 3D CFD, alongside experimental testing, to fully validate the meanline optimization process.
- So far optimization has been aerodynamic-only; no inertia or structural constraints are currently imposed. Future work must consider implications of design changes on turbine inertia, since this affects engine transient response (a critical customer requirement), and blade shape optimization must accommodate mechanical stress constraints, if the methodology is to be commercially useful.
- As mentioned, no engine design parameters have so far been adjusted, but this could reveal further efficiency gains. This will require closer collaboration with the engine manufacturer to perform simultaneous engine and turbocharger optimization.

References

1. Qiu, X. and Baines, N., “Performance Prediction for High Pressure-Ratio Radial Inflow Turbines,” *In* Proc. ASME Turbo Expo, Paper No. GT2007-27057, 2007, doi:10.1115/GT2007-27057.

2. Wasserbauer, C.A. and Glassman, A.J., “FORTRAN Program for Predicting Off-Design Performance of Radial-Inflow Turbines,” NASA Tech. Note D-8063, 1975.

3. Meitner, P.L. and Glassman, A.J., “Computer code for off-design performance analysis of radial-inflow turbines with rotor blade sweep,” AVRADCOM Tech. Rep. 83-C-4, 1983.

4. Baines, N.C., “A meanline prediction method for radial turbine efficiency,” *In* Proc. IMechE 6th Int. Conf. on Turbocharging & Air Management Systems, Paper No. C554/006, 1998.

5. Abidat, M., “Design and testing of a highly loaded mixed flow turbine,” PhD Thesis, University of London, 1991.

6. Romagnoli, A. and Martinez-Botas, R., “Performance prediction of a nozzled and nozzleless mixed-flow turbine in steady conditions,” *Int. J. Mech. Sci.* 53(8):557–574, 2011, doi:10.1016/j.ijmecsci.2011.05.003.

7. Sakellaridis, N. and Hountalas, D., “Meanline Modeling of Radial Turbine Performance for Turbocharger Simulation and Diagnostic Applications,” SAE Technical Paper 2013-01-0924, 2013, doi:10.4271/2013-01-0924.

8. Kapoor, P., Javed, A., and Costall, A., “Optimization of a Radial Turbine Design for Improved Engine-Turbocharger Matching,” *In* Proc. THIESEL Conference on Thermo-and Fluid Dynamic Processes in Direct Injection Engines, pp.1–12, 2014.

9. Romagnoli, A., “Aerodynamic and thermal characterization of turbocharger turbines: experimental and computational evaluation,” PhD Thesis, Imperial College London, 2010.

10. Japikse, D. and Baines, N.C., “Introduction to Turbomachinery,” Concepts ETI, 1997.

11. Whitfield, A. and Baines, N.C., “Design of Radial Turbomachines,” Longman Scientific & Technical, UK, 1990.

12. Yeo, J. H. and Baines, N. C., “Pulsating Flow Behaviour in a Twin-Entry Vaneless Radial-Flow Turbine,” *In* Proc. IMechE 4th Int. Conf. on Turbocharging & Turbochargers, Paper C405/004, 1990.

13. Menter, F.R., “Two-equation eddy-viscosity turbulence models for engineering applications,” *AIAA J.* 32(8):1598–1605, 1994, doi:10.2514/3.12149.

14. Javed, A. and Kamphues, E., “Evaluation of the Influence of Volute Roughness on Turbocharger Compressor Performance From a Manufacturing Perspective,” *In* Proc. ASME Turbo Expo, Paper No. GT2014-26949, 2014, doi:10.1115/GT2014-26949.

15. Mason, A., Costall, A., and McDonald, J., "The Sensitivity of Transient Response Prediction of a Turbocharged Diesel Engine to Turbine Map Extrapolation," SAE Technical Paper 2017-24-0019, 2017, doi:10.4271/2017-24-0019.

16. Goldberg, D.E., “Genetic Algorithms in Search, Optimization, and Machine Learning,” 13th Ed., Addison Wesley Publishing Co., USA, 1989.

17. Petrowski, A. and Hamida Ben, S., “Evolutionary Algorithms,” 1st Ed., John Wiley & Sons, Inc., USA, 2017.

18. Javed, A., “Developing Generic Design Expertise for Gas Turbine Engines: Robust Design of a Micro Centrifugal Compressor,” PhD Thesis, TU Delft, 2014.

19. Khairuddin, U. and Costall, A.W., “Aerodynamic Optimization of the High Pressure Turbine and Interstage Duct in a Two-Stage Air System for a Heavy-Duty Diesel Engine,” ASME *J. Eng. Gas Turbines Power* 140(5):052801–052801-10, 2017, doi:10.1115/1.4038024.

20. Gamma Technologies Inc., “GT-SUITE Optimization Manual,” 2016.

Contact Information

Dr Aaron Costall
Lecturer in Thermofluids
Imperial College London
Department of Mechanical Engineering
South Kensington Campus
London SW7 2AZ
United Kingdom
a.costall@imperial.ac.uk

Acknowledgments

The authors would like to express their thanks to Mitsubishi Turbocharger and Engine Europe BV for funding this project and providing turbine geometrical and performance data, and Groupe Renault for providing the engine model and test data.

Definitions/Abbreviations

Roman symbols

B	blade height
C	absolute velocity
e	tip clearance
i	incidence
K	calibration coefficient
L	enthalpy loss
N	blade number
P	pressure
r	radius
S	swirl loss coefficient
U	blade speed
W	relative velocity
z	blade length

Greek symbols

β	relative flow angle
μ	dynamic viscosity
ρ	density

Subscripts

0	total condition
1	volute inlet
2	rotor inlet
3	rotor outlet
a	axial
b	blade
c	clearance
df	disk friction
i	incidence
max	maximum
min	minimum
opt	optimal
p	passage
r	radial
tip	blade tip
θ	tangential

Abbreviations

BMEP	Brake Mean Effective Pressure
BSFC	Brake Specific Fuel Consumption
BSR	Blade:Speed Ratio
CFD	Computational Fluid Dynamics
GA	Genetic Algorithm
GDI	Gasoline Direct Injection
MTEE	Mitsubishi Turbocharger and Engine Europe BV
RANS	Reynolds-averaged Navier-Stokes
PMEP	Pumping Mean Effective Pressure